Bio-based, cellulosic-CuInS$_2$ nanocomposites for optoelectronic applications

David Reishofer[†], Thomas Rath[†], Heike M. Ehmann[†], Christian Gspan[§], Sebastian Dunst[†], Heinz Amenitsch[ǀ], Harald Plank[§], Bruno Alonso[¥], Emmanuel Belamie[¥], Gregor Trimmel[†], and Stefan Spirk[‡†*]*

[†]*Institute for Chemistry and Technology of Materials, NAWI Graz, Graz University of Technology, Stremayrgasse 9, 8010 Graz, Austria.*

[§]*Graz Centre for Electron Microscopy, Graz University of Technology, Steyrergasse 17, 8010 Graz, Austria.*

[ǀ]*Institute for Inorganic Chemistry, Graz University of Technology, Stremayrgasse 9, 8010 Graz, Austria.*

[¥]*Institut Charles Gerhardt Montpellier, UMR 5253 CNRS/UM/ENSCM, ENSCM-8, rue de l'Ecole Normale, 34296 Montpellier Cedex, France.*

[‡]*Institute for Paper, Pulp and Fiber Technology, Graz University of Technology, Inffeldgasse 23, 8010 Graz, Austria and University of Maribor, Institute for Engineering Materials & Design, Smetanova Ulica 17, 2000 Maribor, Slovenia.*

Members of the European Polysaccharide Network of Excellence (EPNOE)

To whom correspondence should be addressed: stefan.spirk@tugraz.at

1

Abstract

A generic approach to design optoelectronic devices using renewable biopolymers is demonstrated. As a proof of principle, a biopolymer/$CuInS_2$ nanocomponent-based solar cell has been assembled by using a cellulose derivative with a reasonable life cycle performance, namely trimethylsilyl cellulose (TMSC). The solar cells are manufactured using a mixture of copper and indium xanthates as precursors, which decompose and form CIS nanoparticles within the biopolymer matrix during a thermal treatment, which was investigated by *in situ* combined grazing incidence small and wide angle X-ray scattering experiments. The growth of the nanoparticles is thereby controlled by the TMSC matrix. The nanocrystals exhibit an average diameter of approx. 4 nm. Using this composite, it was possible to fabricate solar cells, generating current in a wide range of the solar spectrum and exhibiting power conversion efficiencies of ca. 1%.

Keywords: solar cell, cellulose nanocomposite, trimethylsilyl cellulose, ATR-IR, GISWAXS, copper indium sulfide

Synopsis

Replacement of synthetic, petrochemically-based materials by bio-based renewable feedstocks in the design of optoelectronic devices is exemplary demonstrated at the example of a cellulose derivative.

INTRODUCTION

To meet the challenges of climate change and sustainable use of global resources, tremendous efforts have been made to replace fossil derived energy resources and synthetic petrochemical-based materials by those derived from renewable resources. This development is mainly driven by the rather large CO_2 emissions associated with both, production of energy and of synthetic materials.[1] Among renewable energy resources, photovoltaics are one of the main pillars. One currently followed research area is the use of nanocrystals and nanocomposites in solar cells using at present mainly toxic compounds such as PbS or Cd-based chalcogenides.[2-5] In order to overcome environmental concerns, alternatives have been thoroughly investigated, among which $CuInS_2$ represents a non-toxic alternative.[6-9] However, also in this case, $CuInS_2$ is usually synthesized via wet-chemical/colloidal synthesis routes employing long-chained capping ligands, which have to be removed or exchanged using potentially toxic reagents (e.g. 1,3-benzenedithiol, hexanethiol, etc.) before the nanocrystalline absorber films for the solar cells can be prepared.[10,11] A convenient way to avoid capping agents and ligand exchange reagents is to generate the metal sulfide particles directly in the photovoltaic active layer. In this approach, nanocrystals are formed from precursor compounds which are converted to metal sulfides usually by a mild thermal treatment. Usually, a conjugated polymer matrix is used for controlling the nanocrystal growth.[12] Among the precursors, metal xanthates have proven to be most efficient since they decompose accompanied by the formation of only volatile by-products leaving the layer leading to pure conjugated polymer/nanocrystal nanocomposite thin films which can be directly applied as absorber layers in solar cells.[12-14] In this work, we investigate if it is possible to fully circumvent the use of synthetic capping ligands, ligand exchange reagents and polymers in the fabrication of $CuInS_2$-based nanocrystal solar cells by replacing them in the in-situ route by the bio-based trimethylsilyl cellulose.

3

Particularly cellulose and its derivatives have an enormous potential to substitute conventional polymers from several viewpoints.[15] Cellulose is a major constituent of lignocellulosic plant cell walls, it occurs in algae as well as in fungi and further it is biodegradable. Currently, it is exploited in a wide range of applications ranging from textiles, papermaking, food additives, and in medicine, to mention just the important ones.

Trimethylsilyl cellulose is a particular congener due to several reasons. It is organosoluble (at high degree of substitution with silyl groups), and further it can be easily converted to cellulose by simple exposure to HCl vapors cleaving off the non-toxic side product hexamethyldisiloxane (HDSO).[16] Life cycle analyses from the early 80ies of the last century revealed a good performance of TMSC in fiber spinning applications.[17,18] Later, its ability to form homogenous thin films on different types of surfaces was exploited to generate cellulose interfaces by exposing them to HCl vapors.[16] This opened the door for a fast production of different types of films with high reproducibility having a variety of applications such as photolithographically patterned dielectric gates in thin film transistors.[19] However, nanocomposite thin films derived from TMSC are much less explored. Such films are potentially interesting as model systems for drug release,[20] for the generation of nanoparticle decorated surfaces,[21,22] as well as for thin film membranes.[23]

The use of TMSC instead of synthetic ligands for such purposes follows several principles of the green chemistry (GC) and engineering (GE) principles, namely the use of a renewable feedstock (GC7, and GE12), better recyclability (GE 3, 6, 9, and 11) and enhanced biodegradability (GC10) compared to commonly employed polymers from fossil sources.[1]

MATERIALS AND METHODS

Materials. Trimethylsilyl-cellulose (TMSC; Avicel pulp DS: 2.7-2.9), purchased from TITK Rudolstadt MFSA, copper xanthate (copper O-2,2-dimethylpentan-3-yl-dithiocarbonate, CuXa) and indium xanthate (indium O-2,2-dimethylpentan-3-yl-dithio-carbonate, InXa), synthesized according to a literature procedure[12] , were used as starting materials for the thin film preparation. Chloroform (99 wt%) and sulfuric acid (95 wt%) were purchased from VWR chemicals and hydrogen peroxide (30 wt%) from Sigma-Aldrich. All chemicals were used without purification. Silicon wafers, glass slides (Roth), Au-coated glass slides as substrate (SPR102-AU), Filter Chromafil® Xtra PVDF-45/25 0.45 μm, petri dishes (20 mL; 5 cm diameter), glass/ITO substrates (Xinyan Technology Ltd., Hong Kong) and PEDOT:PSS (Clevios P VP.Al 4083, Heraeus) were used as obtained.

Film preparation. For the characterization of the hybrid material, different substrates (atomic force microscopy, surface free energy, Stylus profilometry, GISWAXS, STEM: silicon wafer (1.4 x 1.4 cm); UV-Vis: glass slides (1.4 x 1.4 cm); ATR-IR: gold coated glass slide (2.0 x 1.0 cm)) were necessary. At the beginning, the substrates were cleaned with "piranha" acid ($H_2SO_4:H_2O_2$ = 7:3 (v/v)) for 30 min (10 min for gold coated glass slides) and rinsed afterwards with distilled water to neutralize the surface. For the film preparation, TMSC (0.5 wt%) was dissolved in $CHCl_3$, filtered and combined (1:1 (v/v)) with the copper and indium xanthate (TMSC:$CuInS_2$ = 1:7 mol) solution (2 wt%, 6 wt%, 12 wt% in $CHCl_3$). This solution (180 μL) was spin coated on the different substrates at 4000 rpm for 60 s (acceleration 2500 rpm/s). The final in-situ synthesis of the $CuInS_2$-nanoparticles ($CuInS_2$-NPs) was done by thermal conversion (195°C over a period of 30 min, heating rate = 10°C/min) of copper and indium xanthate on a programmable heating plate.

ATR-IR spectroscopy. The infrared spectra were recorded with an ALPHA FT-IR spectrometer (Bruker; Billerica, MA, USA). For the measurement an attenuated total reflection (ATR) attachment was used with 48 scans at a resolution of 4 cm^{-1} and a scan range between 4000 and 400 cm^{-1}. The samples were prepared on Au-coated glass slides (SPR102-AU). The data were analyzed with OPUS 4.0 software.

Atomic force microscopy. For the atomic force microscopy (AFM) measurements a Veeco Multimode Quadrax MM AFM (Bruker; Billerica, MA, USA) was used. The images were recorded in the tapping mode (non-contact mode) and silicon cantilevers (NCH-VS1-W from NanoWorld AG, Neuchatel, Switzerland) were used with an average spring constant of 42 N/m (Force Constant) and a resonance frequency of 270 – 320 kHz (Coating: none). All measurements were performed at room temperature and under ambient atmosphere. The image processing and the calculation of the root mean square roughness (calculated from a 6 x 6 µm image) were done with the Nanoscope software (V7.30r1sr3; Veeco).

Profilometry. The determination of the layer thickness was done on a Bruker DekTak XT surface profiler. The scan length was set to 1000 µm over the time duration of 3 seconds. The profile was set to *hills* and *valleys*. The diamond stylus had a radius of 12.5 µm and the force was 3 mg with a resolution of 0.333 µm/sample and a measurement range of 6.5 µm. This measured profile was then used to determine the thickness.

Surface free energy. To determine the static contact angle and the surface free energy (SFE) a drop shape analysis system DSA100 (Krüss GmbH, Hamburg, Germany) with a T1E CCD video camera (25 fps) and the DSA1 v 1.90 software was used. For the measurements 3 µL droplets of Milli-Q water (≥18 MΩcm^{-1}) and diiodomethane as test liquids in the sessile drop modus at 25 °C were deposited on the substrates. The dispense rate was adjusted to 200 µL/min and the time

before the image was captured was 2 seconds. Each sample was measured at least three times. The contact angle (CA) calculations were performed with the Young-Laplace equation and the surface free energy calculation with the Owens-Wendt-Rabel & Kaelble method.

UV-Vis spectroscopy. The UV-Vis absorption spectra of the samples were measured with a Shimadzu UV-1800 UV spectrophotometer. The absorbance was determined from 270 - 1100 nm at 25°C and in ambient atmosphere.

Grazing incidence small and wide angle X-ray scattering. 2D grazing incidence small and wide angle X-ray scattering (GISAXS, GIWAXS) measurements were conducted at the Austrian SAXS Beamline 5.2L of the electron storage ring ELETTRA (Trieste, Italy),[24] using a similar setup as described before.[25] The beamline has been adjusted to a q-resolution (q=4π/λ*sin(2θ/2), 2θ represents the scattering angle) between 0.1 and 3.5 nm^{-1} (GISAXS). The X-ray energy was 8 keV. For the time-resolved measurements, the nanocomposite samples were placed in a heating cell (DHS 1100 from Anton Paar GmbH, Graz, Austria) equipped with a custom-made dome with Kapton polyimide film windows and were heated from 30 °C up to 230 °C at a heating rate of approx. 10 °C min^{-1} under nitrogen atmosphere. During the temperature scan, data were recorded with framing rate of 6 s using a Pilatus 1M detector (Dectris). For detection of the GIWAXS signal, a Pilatus 100K detector from Dectris was used. The angular calibration of the detectors was carried out using silver behenate powder (d-spacing of 58.38 Å) and p-bromo benzoic acid, respectively.

Transmission electron microscopy. Electron diffraction patterns and STEM (Scanning Transmission Electron Microscopy images) were acquired using a Tecnai F20 (operated at 200 kV) and a FEI Titan[3] G2 60-300 (operated at 300 kV). Both microscopes are equipped with a post-column electron energy filter from Gatan Inc. (GIF). The Titan microscope has a Cs probe

corrector for the STEM mode and therefore the high resolution STEM images were observed on the Titan[3] G2 microscope. Selected area electron diffraction patterns (SAED) from the nanoparticles were recorded energy-filtered within a range of about 1400 nm in diameter.

Solar cell assembly. The nanocrystal solar cells were fabricated in the device architecture glass/ITO/PEDOT:PSS/biopolymer-$CuInS_2$/Al. As substrates, glass/ITO slides with a sheet resistance of 10 Ω/sq were used, which were cleaned in deionized water and isopropanol in an ultrasonic bath followed by O_2 plasma cleaning (FEMTO, Diener Electronic, Germany). Afterwards, a PEDOT:PSS layer (Clevios P VP.Al 4083, Heraeus) was doctor blading on the glass/ITO layer in ambient atmosphere and subsequently annealed at 150 °C for 10 min in a glove box. Next, the nanocomposite films were prepared by doctor blading of a chlorobenzene solution containing copper xanthates, indium xanthates and TMSC (concentration of TMSC in the precursor solution: 5 mg/mL; the weight ratio TMSC:$CuInS_2$ was 1:9, the molar ratio CuXa/InXa 1:1.7) and subsequent thermal treatment (temperature program: 15 min heating from room temperature to 195 °C followed by 15 min at 195 °C) on a programmable heating plate (MCS 66, CAT Ingenieurbüro M. Zipperer GmbH). In the last preparation step, approximately 100 nm thick aluminum electrodes were deposited via thermal evaporation at a base pressure of 5×10^{-6} to 1×10^{-5} mbar. The characteristic values of the prepared solar cells were determined from IV curves recorded using a Keithley 2400 SourceMeter, a custom made Lab-View software and a Dedolight DLH400D lamp providing a spectrum very similar to AM1.5G. The light intensity was set to 100 mW/cm^2 (determined using a KippZonen-CMP-11 pyranometer, no spectral mismatch was considered). The EQE spectrum was measured using a Multimode4 monochromator (AMKO) equipped with a Xenon lamp and a Keithley 2400 source meter.

Results and Discussion

The aim of this paper is to design a nanocrystal solar cell based on $CuInS_2$ and TMSC. In order to realize this goal (Scheme 1), different requirements must be met, namely solvent compatibility between the xanthate precursors and TMSC (i), the formation of homogeneous precursor films by spin-coating these solutions onto PEDOT:PSS/ITO (ii), the conversion of the metal xanthates to the metal sulfide nanoparticles in the TMSC matrix (iii), the final assembly of the device (iv) and finally the determination of the photoelectric activity of the assembled solar cells (v). In all these steps, comprehensive characterization techniques are employed to investigate the underlying processes.
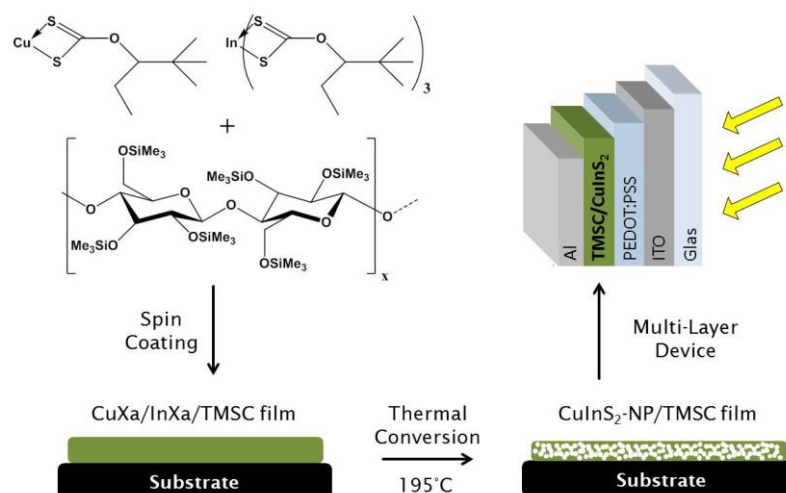

Scheme1. Schematic representation of the manufacturing steps of $CuInS_2$/TMSC nanocomposite films and the multi-layer optoelectronic device.

As mentioned above, solvent compatibility between the xanthates and TMSC needs to be ensured. Based on previous findings in literature to prepare $CuInS_2$ nanoparticles, the ratio between the two xanthates (CuXa/InXa) was fixed at 1.0:1.7.[12] Then, a solubility screening was performed. For this purpose, different amounts of CuXa/InXa (2-12 wt% in chloroform) were added to TMSC solutions (0.5 wt%). All concentrations resulted in clear yellow-brownish

solutions. These solutions were further subjected to spin-coating experiments and all the ratios led to films with a rather smooth optical appearance. Afterwards, the nanoparticle growth was induced by exposing the films to elevated temperature (195 °C, up to for 230 °C for GISWAXS). Decomposition of the xanthates via the Chugaev rearrangement[26] is initiated at a temperature of around 155 °C as shown earlier.[12] A benefit provided by the TMSC derivative is the rather high thermal stability (degradation starts at 280 °C, see Fig. S1, ESI†).

The influence of the heating step on the chemical composition of the films was monitored by ATR-IR spectroscopy. **Fig. 1** compares the different materials before and after the heating procedure. The obtained results revealed that the TMSC was neither altered by exposure to elevated temperature (e.g. no hydrolysis indicated by the appearance of OH bands associated to ν_{OH} at 3200-3600 cm^{-1}) nor by the addition of copper or indium xanthate. Furthermore, it is demonstrated that the heating step led to decomposition of both xanthates while the TMSC remains unaffected.
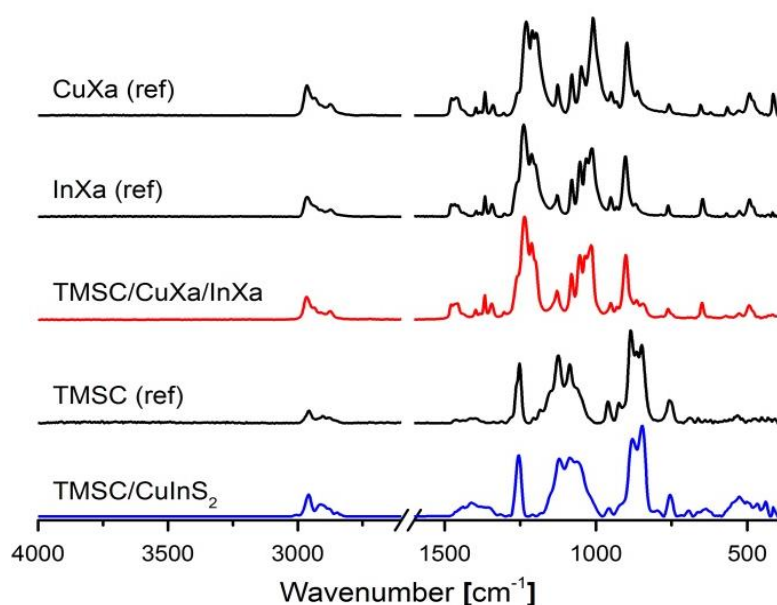
Figure 1. Comparison of ATR-IR spectra of the pure films (CuXa, InXa and TMSC) with nanocomposite thin films before and after heating to 195°C at a CuXa/InXa ratio of 1:1.7 and a concentration of 12 wt%.

For the non-treated TMSC/CuXa/InXa film, characteristic bands for the xanthates as well as those for the TMSC were detected. The bands at 1081, 1054 and 1016 cm^{-1} can be assigned to C-S stretching vibrations and those at 1237 and 1212 cm^{-1} to asymmetric C–O–C stretching vibrations of the metal xanthates.[27, 28] The bands associated to the TMSC matrix are present at 848 cm^{-1} which is characteristic for ν_{Si-C}. After the heat treatment, all bands associated with CuXa and InXa vanished, indicating the decomposition of the xanthates and the formation of CuInS$_2$ nanoparticles. The remaining bands (1255, 1119, 1086, 880, 848 cm^{-1}) are distinct for Si-C and Si-O-C vibrations of TMSC. Moreover, these results prove that the TMSC is not regenerated to cellulose and remain untouched during the in-situ synthesis of the nanoparticles at 195°C.

In order to get insights into the formation of the CuInS$_2$ nanocrystals in the TMSC matrix, we conducted combined time resolved GIWAXS and GISAXS experiments using synchrotron radiation on a temperature controlled sample stage. The temperature-dependent evolution of the GIWAXS patterns of a TMSC/metal xanthate sample is shown in **Fig. 2**. Between 120 and 150 °C, an intense broad peak between 26 and 32° and a minor one around 47° 2 theta evolved. These peaks can be assigned to the (112) and (204) reflections, which are characteristic for chalcopyrite CuInS$_2$. Therefore, it can be concluded that the conversion of the precursors to the CuInS$_2$ nanocrystals takes place within this temperature range. The corresponding GIWAXS patterns are shown in the SI (Fig. S3; ESI†) in higher time resolution. Further, time-resolved GISAXS measurements were performed using 100 nm thick films and a time resolution of 6 s.
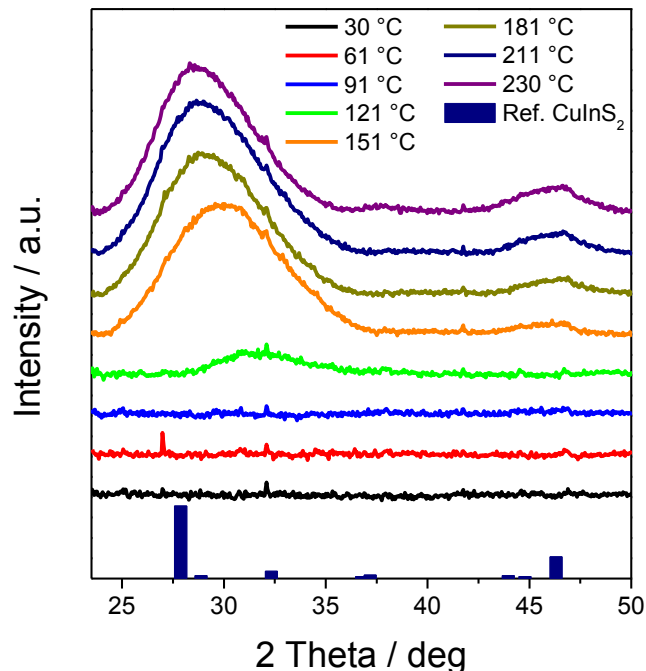
Figure 2. Evolution of the GIWAXS patterns of a TMSC/metal xanthate sample during the heating run (the data are shifted horizontally for better visibility) and a reference pattern of tetragonal $CuInS_2$ (PDF 032-0339).

These short intervals are beneficial as the formation of nanocrystalline metal sulfides from metal xanthates proceeds rather fast.[29, 30] The GISAXS patterns at selected temperatures during the heating run are presented in **Fig. 3A** demonstrating a strong increase of scattering due to the formation of $CuInS_2$ particles. The areas used for horizontal integration are indicated with a red box in the GISAXS images and the resulting horizontal cuts at $q_z = 0.45$ nm^{-1} are presented in **Fig. 3B**.

The evolution of the integrated intensities of the GISAXS patterns (**Fig. 3C**), calculated between q_y=0.1 and 2.5 nm^{-1}) revealed that minor structural changes were taking place in the TMSC/metal xanthate film already starting at a temperature of around 120 °C. At approx. 145-150 °C, a significant increase in the integrated intensity was observed. This originated from the

decomposition of the metal xanthates, the evaporation of volatile organic decomposition products and the formation of $CuInS_2$ nanocrystals in this temperature range as already revealed by the GIWAXS investigations. By these processes, the overall electron density in the nanocomposite film was increased, leading to an enhanced scattering intensity in the GISAXS patterns. After the formation of the $CuInS_2$ nanocrystals, the changes in the integrated intensities were minor. Any evidence for further compaction of the nanocomposite film and decomposition of the organic TMSC matrix was not observed until a temperature of 230 °C.
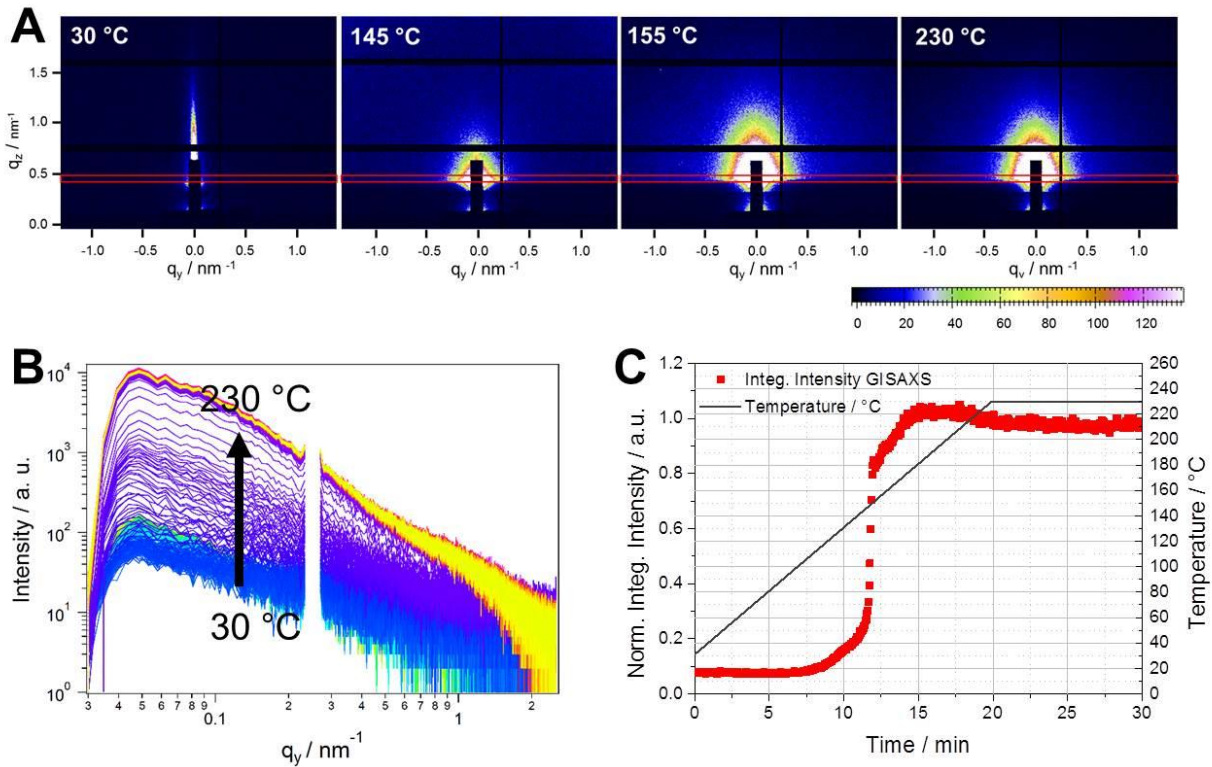
Figure 3. (A) GISAXS images of a TMSC/metal xanthate sample at different temperatures during the formation of the $CuInS_2$ nanocrystals in the TMSC matrix (the red boxes indicate the areas used for horizontal integration), (B) temperature-dependent evolution of the horizontal cuts of the GISAXS patterns and (C) the corresponding integrated intensities of the GISAXS curves.

13

A further important point for the usage of the nanocomposite layers in a solar cell or other optoelectronic devices is the connection of the separate nanoparticles inside the film to ensure a continuous pathway allowing for electronic conduction throughout the material. The bright field TEM images at different magnifications (**Fig. 4A, B**) revealed a dense network of nanoparticles with diameters from 2 nm to 5 nm in the TMSC matrix. Also here crystallographic data on the nanoparticles' structure can be derived by selected area electron diffraction patterns (SAED) (**Fig. 4C**)). The diffraction patterns feature three main diffraction rings at r = 3.18 nm^{-1} (112), r = 5.16 nm^{-1} (204/220) and r = 6.01 nm^{-1} (116/312) which are in excellent agreement with reference data for chalcopyrite $CuInS_2$ (PDF 032-0339) and a proof for the high crystallinity of the nanoparticles inside the film.
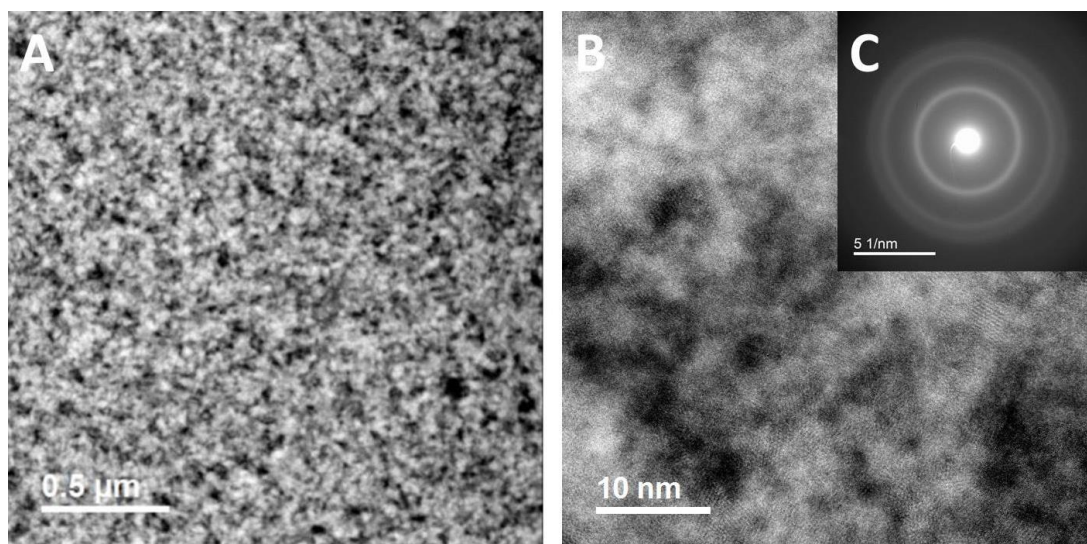
**Figure 4.** Images (A) and (B) represent bright field TEM images of a sample having 12 wt% $CuInS_2$-NP in a TMSC matrix at different magnifications and (C) a corresponding SAED image. More data is available in the ESI† (Fig. S4).

An important aspect for the design of optoelectronic devices is the morphology of the hybrid layer. Especially in the assembly of multi-layer devices, the surface roughness of the different

layers is crucial for their performance. For that reason the surface was analyzed by atomic force microscopy (AFM) before and after the heat treatment.
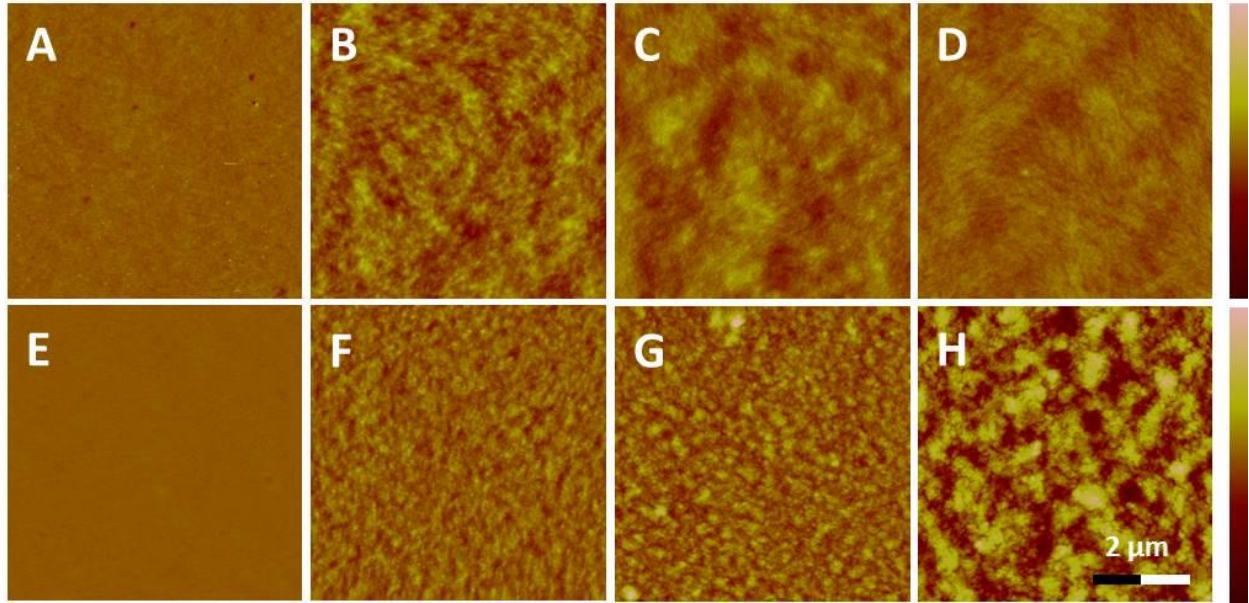
Figure 5. AFM images of the different films. Upper row: untreated, A) TMSC matrix, B) 2 wt%, C) 6 wt%, D) 12 wt% TMSC/CuXa/InXa, Z-scale (A, B, C, D) = 40 nm; bottom row: heat treated, E) TMSC matrix heat treated, F) 2 wt%, G) 6 wt% H) 12 wt% TMSC/CuInS$_2$, Z-scale (E, F, G, H) = 100 nm

Fig. 5 shows the results of the AFM measurements, which reveal a smooth surface for the untreated films (A – D). This can be explained with the good solubility of the starting materials and the good film forming properties of the material. Compared with the pure TMSC reference sample, the TMSC/CuXa/InXa films had some small surface features, but they did not influence the surface roughness (~ 2 nm). Furthermore, also the concentration of CuXa/InXa did not have a significant impact on the morphology. After the heat treatment, the topography of the surface changed and the surface roughness increased, which correlated to the amount of nanoparticles. The surface roughness was 4.4 nm for the lowest concentration (2 wt%), 6.1 nm (6 wt%) and

12.8 nm at 12 wt%. These values imply that the surface is smooth enough for the envisaged use in solar cell applications. During the heat treatment, the film thickness decreased due to the removal of volatile compounds of the xanthates from 220 ± 6 to 76 ± 3 nm (2 wt%), 625 ± 7 to 105 ± 2 nm (6 wt%) and 1241 ± 12 to 193 ± 5 nm for 12 wt%. During the heating process the films lost 65 – 84% of their initial thickness due to the decomposition of the xanthates and the related higher packing density of the $CuInS_2$ nanoparticles.

For the usage in a multi-layer device like a solar cell the wettability of the nanocomposite is important. Especially, the surface free energy (SFE), calculated by contact angle measurements of at least two liquids (H_2O, CH_2I_2; Fig. S5 and S6, ESI†), is a crucial parameter whose tuning allows for preventing adhesion problems with connecting layers.

The hydrophobic character of the TMSC/CuXa/InXa film was reflected in a water contact angle of approximately ~97° and a surface free energy of 18-23 mJ/m² with a major apolar contribution. After the heat treatment and the associated formation of $CuInS_2$ nanoparticles, the films retain their hydrophobic character (CA ~90°). Simultaneously, the surface free energies increased depending on the nanoparticle concentration. This effect may originate from roughness effects since SFE increases with increasing $CuInS_2$-NP concentrations in the films. Moreover, these data also confirm the stability of the TMSC during the heat treatment regardless of the starting xanthate concentration.

The UV-VIS absorption of the film was determined to prove the suitability of the hybrid material for the application as an absorber material in a nanocrystal solar cell. The untreated film showed a distinctive absorption band for CuXa/InXa starting at ca. 420 nm, which vanished after the heat treatment (see **Fig. 6**). At the same time, the characteristic spectrum of $CuInS_2$ nanoparticles with

an onset between 800-900 nm appeared.[12] Furthermore, the TMSC matrix did not show any absorption in the measured range and did not affect the absorption of the $CuInS_2$ nanoparticles.
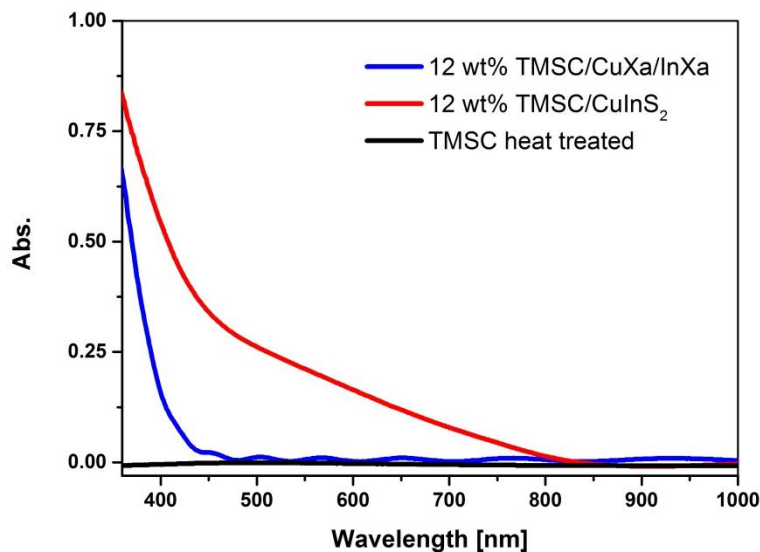
Figure 6. UV-VIS absorption spectra of the 12 wt% untreated, heat treated and TMSC reference sample.

To demonstrate the suitability of the prepared $TMSC/CuInS_2$ films for the application in optoelectronic devices, we prepared solar cells using a simple device architecture by sandwiching the $TMSC/CuInS_2$ films between ITO/PEDOT:PSS and aluminum electrodes. In **Fig. 7A**, typical IV curves for such a device measured in the dark and under illumination are shown. The solar cell exhibited a V_{OC} of 480 mV, which is in line with other reported solar cells based on nanocrystalline $CuInS_2$/conjugated polymer absorber films.[6] The short circuit current was approximately 5.5 mA/cm². This is significantly lower compared to solar cells with absorber layers in which $CuInS_2$ nanocrystals are embedded in a matrix of a conjugated polymer.[12] However, the observed I_{SC} proves that an interconnected network of $CuInS_2$ nanocrystals was formed in the insulating TMSC matrix allowing for efficient charge transport in the nanoparticle

17

phase to the electrodes. While the control of nanocrystal growth and film formation can be challenging in the formation of nanocrystal solar cells, here the TMSC matrix seems to prevent extensive growth of the nanoparticles during the formation, facilitates the formation of a homogeneous thin film and inhibits short circuiting of the device. Overall, a power conversion efficiency of 0.99% was obtained by the *in situ* prepared TMSC/CuInS$_2$ absorber films. An EQE spectrum of a TMSC/CuInS$_2$ solar cell is shown in **Fig. 7B** (for the IV curves of this solar cell, see Fig. S7, ESI†). The onset in the EQE spectrum is around 850 nm, which matches well with the optical bandgap of CuInS$_2$ and the absorption onset of the TMSC/CuInS$_2$ layer. Further information on the cross section (by FIB-SEM) is available in Fig. S8 (ESI†).
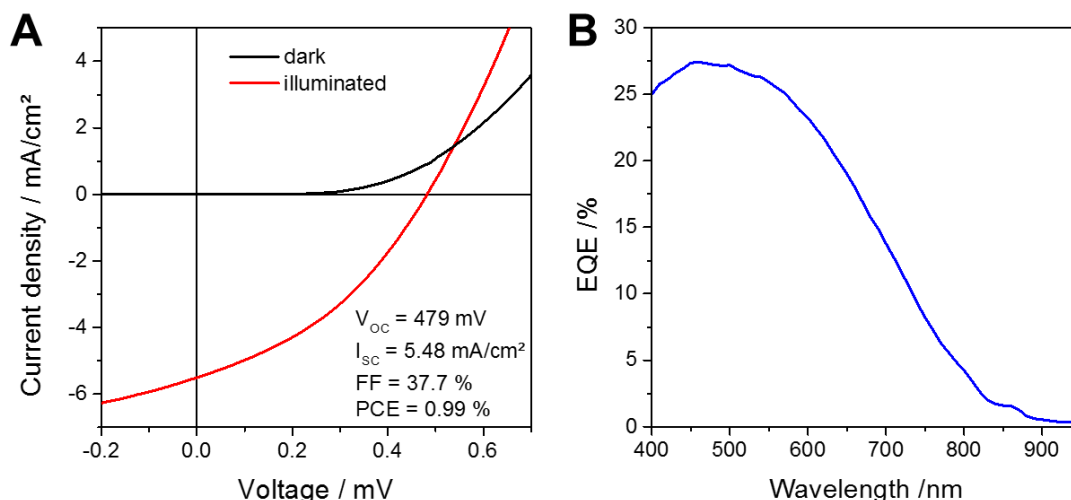
Figure 7. (A) IV curves measured in the dark and under 100 mW/cm² illumination and (B) an EQE spectrum of a CuInS$_2$/TMSC solar cell.

Further, the chosen approach is in principle scalable to other biopolymers as well, as long as they form stable films, which are not decomposed by the heat treatment required for the generation of the nanoparticles. At the moment, we explore chitin nanocrystals (ChNCs) derived films for such purposes as well. **Fig. 8A** illustrates a comparison of the ATR-IR spectra of ChNCs/CuInS$_2$-

nanocomposite with the precursor film ChNCs/CuXa/InXa as well as the pure reference materials CuXa, InXa, and ChNCs. The spectrum of the final ChNCs/CuInS$_2$-nanocomposite is dominated by the vibrations of the ChNCs, whereas the significant peaks from the xanthate precursors are absent proving complete conversion to CuInS$_2$.
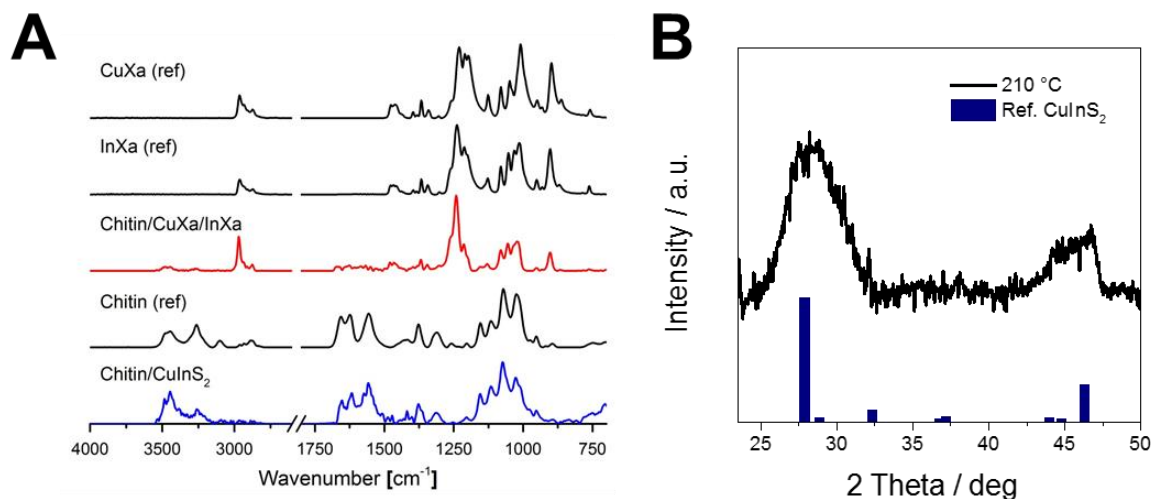
Figure 8. a) Comparison of the ATR-IR reference spectra (CuXa, InXa and chitin) with nanocomposite thin films having a CuXa/InXa (1:1.7) concentration of 3.7 wt%; b) GIWAXS pattern of the final ChNC/CuInS$_2$-nanocomposite and a reference pattern of tetragonal CuInS$_2$ (PDF 032-0339).

The formation of CuInS$_2$ - investigated again by combined GIWAXS and GISAXS experiments - takes place at slightly higher temperatures of approx. 170 °C (see Figures S11 and S12, ESI†) compared to the conversion to the CuInS$_2$ nanocrystals in the TMSC matrix. **Fig. 8B** shows the final GIWAXS trace (measured at 210 °C) in comparison to the CuInS$_2$ reference pattern proving also the formation of CuInS$_2$ in this system. However, the dispersability and the stability upon heat treatment have been shown insufficient so far to prepare a working solar cell with satisfying performance. Especially the obtained high roughness (see AFM images in Figure S9 in the ESI†)

is detrimental for thin film solar cells. Nevertheless, this approach might be interesting for templated porous metal sulfide films analogous to porous silicates obtained by ChNCs-templating.[31]

In summary, we successfully demonstrated the replacement of synthetic ligands by the use of a biopolymer derivative, namely trimethylsilyl cellulose, for the fabrication of $CuInS_2$ nanocrystal solar cells. The solar cells feature a promising power conversion efficiency given the fact that we intended a proof of principle study and any extensive optimization steps of the solar cells were not performed. Further optimization by increasing the nanocrystal content in the biopolymer matrix, its layer thickness, and the incorporation of interlayers, might lead to competitive solar cells with similar or superior performance than the most efficient $CuInS_2$ nanocrystal-based solar cells reported so far.[7-9]

Acknowledgements

Associated Content

Supporting Information. TGA of the used TMSC, supplementary IR spectra, contact angle/surface free energy data, SAED data, additional GISAXS/GIWAXS data, FIB-SEM cross section of the device (Fig. S1-S12).

References

(1) Tabone, M. D.; Cregg, J. J.; Beckman, E. J.; Landis, A. E., Sustainability Metrics: Life Cycle Assessment and Green Design in Polymers. *Environ. Sci. Technol.* **2010,** *44*, 8264-8269.

(2) Yang, J.; Wang, J.; Zhao, K.; Izuishi, T.; Li, Y.; Shen, Q.; Zhong, X., CdSeTe/CdS Type-I Core/Shell Quantum Dot Sensitized Solar Cells with Efficiency over 9%. *J. Phys. Chem. C* **2015,** *119*, 28800-28808.

(3) Ren, Z.; Wang, J.; Pan, Z.; Zhao, K.; Zhang, H.; Li, Y.; Zhao, Y.; Mora-Sero, I.; Bisquert, J.; Zhong, X., Amorphous TiO2 Buffer Layer Boosts Efficiency of Quantum Dot Sensitized Solar Cells to over 9%. *Chem. Mater.* **2015,** *27*, 8398-8405.

(4) Chuang, C.-H. M.; Brown, P. R.; Bulović, V.; Bawendi, M. G., Improved performance and stability in quantum dot solar cells through band alignment engineering. *Nat. Mater.* **2014,** *13*, 796-801.

(5) Yuan, M.; Liu, M.; Sargent, E. H., Colloidal quantum dot solids for solution-processed solar cells. *Nature Energy* **2016,** *1*, 16016.

(6) So, D.; Pradhan, S.; Konstantatos, G., Solid-state colloidal CuInS2 quantum dot solar cells enabled by bulk heterojunctions. *Nanoscale* **2016,** *8*, 16776-16785.

(7) Jara, D. H.; Yoon, S. J.; Stamplecoskie, K. G.; Kamat, P. V., Size-Dependent Photovoltaic Performance of CuInS$_2$ Quantum Dot-Sensitized Solar Cells. *Chem. Mater.* **2014,** *26*, 7221-7228.

(8) Guijarro, N.; Guillen, E.; Lana-Villarreal, T.; Gomez, R., Quantum dot-sensitized solar cells based on directly adsorbed zinc copper indium sulfide colloids. *Phys. Chem. Chem. Phys.* **2014,** *16*, 9115-9122.

(9) Pan, Z.; Mora-Seró, I.; Shen, Q.; Zhang, H.; Li, Y.; Zhao, K.; Wang, J.; Zhong, X.; Bisquert, J., High-Efficiency "Green" Quantum Dot Solar Cells. *J. Am. Chem. Soc.* **2014,** *136*, 9203-9210.

(10) Scheunemann, D.; Wilken, S.; Parisi, J.; Borchert, H., Towards depleted heterojunction solar cells with CuInS$_2$ and ZnO nanocrystals. *Appl. Phys. Lett.* **2013,** *103*, 133902.

(11) Halpert, J. E.; Morgenstern, F. S. F.; Ehrler, B.; Vaynzof, Y.; Credgington, D.; Greenham, N. C., Charge Dynamics in Solution-Processed Nanocrystalline CuInS$_2$ Solar Cells. *ACS Nano* **2015,** *9*, 5857-5867.

(12) Rath, T.; Edler, M.; Haas, W.; Fischereder, A.; Moscher, S.; Schenk, A.; Trattnig, R.; Sezen, M.; Mauthner, G.; Pein, A.; Meischler, D.; Bartl, K.; Saf, R.; Bansal, N.; Haque, S. A.; Hofer, F.; List, E. J. W.; Trimmel, G., A Direct Route Towards Polymer/Copper Indium Sulfide Nanocomposite Solar Cells. *Adv. Energy Mat.* **2011,** *1*, 1046-1050.

(13) Fradler, C.; Rath, T.; Dunst, S.; Letofsky-Papst, I.; Saf, R.; Kunert, B.; Hofer, F.; Resel, R.; Trimmel, G., Flexible polymer/copper indium sulfide hybrid solar cells and modules based on the metal xanthate route and low temperature annealing. *Sol. Energy Mater. Sol. Cells* **2014,** *124*, 117-125.

(14) Arar, M.; Gruber, M.; Edler, M.; Haas, W.; Hofer, F.; Bansal, N.; Reynolds, L. X.; Haque, S. A.; Zojer, K.; Trimmel, G.; Rath, T., Influence of morphology and polymer:nanoparticle ratio on

device performance of hybrid solar cells—an approach in experiment and simulation. *Nanotechnology* **2013,** *24*, 484005.

(15) Klemm, D.; Heublein, B.; Fink, H.-P.; Bohn, A., Cellulose: Fascinating Biopolymer and Sustainable Raw Material. *Angew. Chem. Int. Ed.* **2005,** *44*, 3358–3393.

(16) Schaub, M.; Wenz, G.; Wegner, G.; Stein, A.; Klemm, D., Ultrathin films of cellulose on silicon wafers. *Adv. Mater.* **1993,** *5*, 919-922.

(17) Cooper, G. K.; Sandberg, K. R.; Hinck, J. F., Trimethylsilyl cellulose as precursor to regenerated cellulose fiber. *Journal of Applied Polymer Science* **1981,** *26*, 3827-3836.

(18) Greber, G.; Paschinger, O., Silylderivate der Cellulose. *Lenz. Ber.* **1983,** *55*, 20-25.

(19) Wolfberger, A.; Petritz, A.; Fian, A.; Herka, J.; Schmidt, V.; Stadlober, B.; Kargl, R.; Spirk, S.; Griesser, T., Photolithographic patterning of cellulose: a versatile dual-tone photoresist for advanced applications. *Cellulose* **2015,** *22*, 717-727.

(20) Maver, T.; Maver, U.; Mostegel, F.; Griesser, T.; Spirk, S.; Smrke, D. M.; Stana-Kleinschek, K., Cellulose based thin films as a platform for drug release studies to mimick wound dressing materials. *Cellulose (Dordrecht, Neth.)* **2015,** *22*, 749-761.

(21) Taajamaa, L.; Rojas, O. J.; Laine, J.; Yliniemi, K.; Kontturi, E., Protein-assisted 2D assembly of gold nanoparticles on a polysaccharide surface. *Chem. Commun.* **2013,** *49*, 1318-1320.

(22) Breitwieser, D.; Kriechbaum, M.; Ehmann, H. M. A.; Monkowius, U.; Coseri, S.; Sacarescu, L.; Spirk, S., Photoreductive generation of amorphous bismuth nanoparticles using polysaccharides – Bismuth–cellulose nanocomposites. *Carbohydr. Polym.* **2015,** *116*, 261-266.

(23) Puspasari, T.; Yu, H.; Peinemann, K.-V., Charge- and Size-Selective Molecular Separation using Ultrathin Cellulose Membranes. *ChemSusChem* **2016,** *9*, 2908-2911.

(24) Amenitsch, H.; Rappolt, M.; Kriechbaum, M.; Mio, H.; Laggner, P.; Bernstorff, S., First performance assessment of the small-angle X-ray scattering beamline at ELETTRA. *Journal of Synchrotron Radiation* **1998,** *5*, 506-508.

(25) Fischereder, A.; Rath, T.; Haas, W.; Amenitsch, H.; Schenk, D.; Zankel, A.; Saf, R.; Hofer, F.; Trimmel, G., Investigation of $CuInS_2$ Thin Film Formation by a Low-Temperature Chemical Deposition Method. *ACS Appl. Mater. Interfaces* **2012,** *4*, 382-390.

(26) Pradhan, N.; Katz, B.; Efrima, S., Synthesis of High-Quality Metal Sulfide Nanoparticles from Alkyl Xanthate Single Precursors in Alkylamine Solvents. *J. Phys. Chem. B* **2003,** *107*, 13843-13854.

(27) Socrates, G., *Infrared Characteristic Group Frequences, Tables and Charts*. 2nd ed.; Wiley: Chichester, 1994.

(28) Barreca, D.; Gasparotto, A.; Maragno, C.; Seraglia, R.; Tondello, E.; Venzo, A.; Krishnan, V.; Bertagnolli, H., Synthesis and characterization of zinc bis(O-isopropylxanthate) as a single-source chemical vapor deposition precursor for ZnS. *Appl. Organomet. Chem.* **2005,** *19*, 1002-1009.

(29) Dunst, S.; Rath, T.; Radivo, A.; Sovernigo, E.; Tormen, M.; Amenitsch, H.; Marmiroli, B.; Sartori, B.; Reichmann, A.; Knall, A.-C.; Trimmel, G., Nanoimprinted comb structures in a low bandgap polymer: thermal processing and their application in hybrid solar cells. *ACS Appl. Mater. Interfaces* **2014,** *6*, 7633-7642.

(30) MacLachlan, A. J.; Rath, T.; Cappel, U. B.; Dowland, S. A.; Amenitsch, H.; Knall, A. C.; Buchmaier, C.; Trimmel, G.; Nelson, J.; Haque, S. A., Polymer/nanocrystal hybrid solar cells: Influence of molecular precursor design on film nanomorphology, charge generation and device performance. *Adv. Funct. Mater.* **2015,** *25*, 409-420.
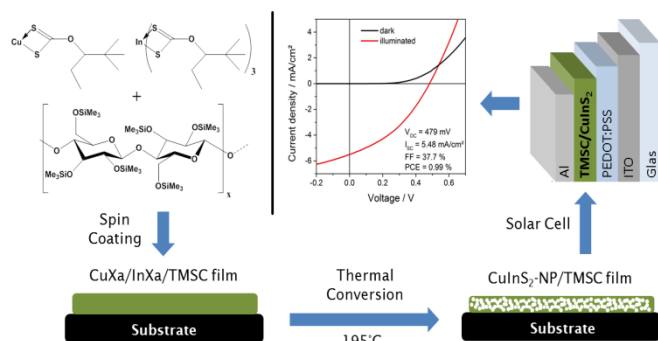
(31) Alonso, B.; Belamie, E., Chitin–Silica Nanocomposites by Self-Assembly. *Angew. Chem. Int. Ed.* **2010,** *49*, 8201-8204.

For Table of Contents Use Only.

Bio-based, cellulosic-CuInS$_2$ nanocomposites for optoelectronic applications

David Reishofer, Thomas Rath, Heike M. Ehmann, Christian Gspan, Sebastian Dunst, Heinz

Amenitsch, Harald Plank, Bruno Alonso, Emmanuel Belamie, Gregor Trimmel, and Stefan Spirk

Synopsis

Replacement of synthetic, petrochemically-based materials by bio-based renewable feedstocks in the design of optoelectronic devices is exemplary demonstrated at the example of a cellulose derivative.